Accepted Manuscript

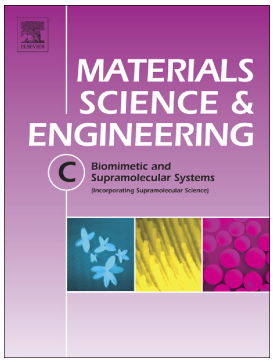

Development and evaluation of novel nanophotosensitizers as photoantimicrobial agents against Staphylococcus aureus

M.S. Gualdesi, V. Aiassa, J. Vara, C.I. Alvarez Igarzabal, C.S. Ortiz

PII: S0928-4931(17)34463-6
DOI: doi:10.1016/j.msec.2018.09.040
Reference: MSC 8903

To appear in: *Materials Science & Engineering C*

Received date: 14 November 2017
Revised date: 14 August 2018
Accepted date: 12 September 2018

Please cite this article as: M.S. Gualdesi, V. Aiassa, J. Vara, C.I. Alvarez Igarzabal, C.S. Ortiz , Development and evaluation of novel nanophotosensitizers as photoantimicrobial agents against Staphylococcus aureus. Msc (2018), doi:10.1016/j.msec.2018.09.040

Development and evaluation of novel nanophotosensitizers as photoantimicrobial agents against *Staphylococcus aureus*

M.S. Gualdesi[1], V. Aiassa[1a], J. Vara[1a], C.I. Alvarez Igarzabal[2], C.S. Ortiz[1]*

[1]Departamento de Ciencias Farmacéuticas, Facultad de Ciencias Químicas, Universidad Nacional de Córdoba. [a]UNITEFA-CONICET, Argentina.

[2]Departamento de Química Orgánica, Facultad de Ciencias Químicas, Universidad Nacional de Córdoba. IPQA-CONICET, Argentina.

*Corresponding author: Tel.: +54 3515353865; fax: +54 3515353364. E-mail address: crisar@fcq.unc.edu.ar (C.S. Ortiz).

Keywords

Antimicrobial photodynamic therapy

Monobrominated neutral red

Monobrominated azure B

Polyacrylamide nanoparticles

Staphylococcus aureus

Abstract

The main aim of the present study was to synthetize polyacrylamide nanoparticles and to use them as photosensitizer carriers. The new monobrominated derivatives (monobrominated neutral red and monobrominated azure B) were the photosensitizers used for antimicrobial photodynamic therapy. They were loaded into the nanocarriers and their antibacterial and oxidative activities were evaluated. The polyacrylamide nanoparticles were evaluated and prepared by inverse microemulsion polymerization. The nanoparticles obtained were characterized by size, polydispersity index, and zeta potential analysis. The Dynamic Light Scattering indicated that the diameter of the particle (z-average) was optimal, with an acceptable polydispersity index. The antibacterial activity of the polyacrylamide nanoparticles loaded with photosensitizers was evaluated against *Staphylococcus aureus*. Both photosensitizers loaded into the nanoparticles showed great potential as antibacterial agents since they suppressed the bacterial growth. The maximum percentage of growth reduction was 35.5% (> 2 Log CFU/mL), with the monobrominated azure B loaded into the nanocarrier with 2 hydroxyethyl methacrylate against methicillin resistant *S. aureus*. The improved physicochemical and photophysical properties of these photosensitizers were accompanied by a significant increase in the photoantimicrobial action, in conventional-sensitive and-methicillin resistant *S. aureus*.

The results obtained clearly suggest that polyacrylamide nanoparticles loaded with photosensitizers have great potential for further application in antimicrobial photodynamic therapy.

1. Introduction

A potential strategy to overcome the antibiotic resistance of numerous microorganisms may be the use of antimicrobial photodynamic therapy (APDT) that employs a localized, light-activated Photosensitizer (PS) that is capable of transferring the energy absorbed to other compounds that, in turn, generate metastable species that are very reactive, particularly singlet oxygen ($^1O_2$), which destroys target cells. The APDT eliminates the bacteria without inducing antibiotic resistance or even requiring daily dosing [1,2]. In contrast to antibiotics, sub-inhibitory doses of PS used in APDT have failed to induce genomic mutations and elevate photodynamic resistance.

The main advantages of APDT are the few side effects, the prevention of the regrowth of the microorganisms after treatment, and the lack of development of resistance mechanisms due to the mode of action and type of biochemical targets (multi-target process). This therapeutic alternative includes noninvasive nature, repeatability without cumulative toxicity, and improved quality of life of the patients [3,4].

Two oxidative mechanisms of photoinactivation are considered to be implicated in the inactivation of the target cells by APDT. The type I pathway involves electron/hydrogen atom-transfer reactions from the PS triplet state with the participation of a substrate to produce radical ions, while the type II pathway involves energy transfer from that triplet state to molecular oxygen to produce $^1O_2$. Both processes lead to highly toxic reactive oxygen species (ROS), able to irreversibly alter vital components of cells, resulting in oxidative lethal damage. ROS causes oxidative stress in the cells, inducing cell death by apoptosis, necrosis or a combination thereof [3].

The new cationic PSs, monobrominated Neutral Red (NRBr) and monobrominated Azure B (AzBBr), were synthesized and characterized in our laboratory (**Fig. 1A**) [5,6].

NRBr proved to have the potential to be used as a PS because it presents less aggregation in different solvents and improved photoproperties, exhibiting significant increases in the photoantimicrobial action compared to Neutral Red [7]. However, this monobrominated derivative proved to be very chemically unstable under physiological conditions. So, it becomes a good candidate to be carried in a drug transporter system.

AzBBr demonstrated an increase in $^1O_2$ yields and a lower efficiency in inactivating cultured tumor cells. The decrease in photodynamic activity was related to an aggregation effect in comparison with the parent compound [5]. Despite its disadvantages, AzBBr is an excellent candidate to produce photocytotoxicity in biological media; therefore, we propose to continue studying it as a third generation PS.

In this way, the new brominated compounds could be included in vehiculization systems in order to improve their properties and increase the phototoxicity. The nanoparticles (NPs) as an emerging technology have the capability to overcome most of the limitations of classical PSs. The fact that most effective PSs tend to be insoluble, hydrophobic molecules with a high propensity to aggregate, means that encapsulation in nano-drug carriers may make a big difference to their performance [8]. The NPs loaded with PSs have been used as carriers to transport PSs into microorganisms and improve antimicrobial performance; particular attention has been paid to biocompatible and biodegradable matrixes [9-13]. Various organic nanomaterials such as liposomes, polymeric NPs, natural macromolecule NPs, as well as a number of other functional NPs with interesting chemical and physical properties have been investigated, showing encouraging results *in vitro* and *in vivo* [8,14-16].

The NPs containing PSs have several advantages over free PSs: transport high concentrations of PS for the production of lethal reactive oxygen species, reduce the ability of the target cell to pump out the PS, decrease the possibility of multidrug resistance, and increase selectivity of treatment by localized delivery agents. In addition, the nanoparticle matrix is non-immunogenic, stopping the aggregation of PS as occurs in the free state and the encapsulation can be used to enhance solubility if the PS is not soluble in water [12,14]. The efficiency of NPs in APDT may be attributed to the fact that this therapy relies on the production of ROS. Therefore, it is unnecessary to release the loaded PS and no time for biodegradation is needed, but it is only essential that the reactive species diffuse in and out of the NP [17].

Polymeric NPs have been widely investigated for their chemical, physical, and structural properties that enable them to be widely applied in drug entrapment, medical imaging, diagnosis, and treatment. Additionally, polymeric nanocarriers may be prepared from natural polymers such as albumin, hyaluronic acid, and chitosan and from synthetic polymers such as polylactic acid, poly glycolic acid, poly (lactide-co-glycolide), polypeptide, and polyacrylamide (PAA) [18]. PAA is an important water-soluble polymer with a large number of acetylamine groups on its macromolecular chains. Recent accelerated biodegradation studies demonstrated the biodegradability of the PAA nanomaterials [19]. The PAA nanoparticle matrix, generally a porous hydrogel, protects the embedded active form of PSs from enzymatic or environmental degradation and permits $^1O_2$ and other kinds of ROS diffusion through the pores.

In view of the above-mentioned facts, in this study, a nanocarrier strategy was developed using biocompatible polymers to incorporate the PSs, NRBr, and AzBBr. In addition, the entrapment of these PSs in novel nanoparticles could offer therapeutic advantages in comparison to free PS active agents since it could prevent different adverse effects.

The nanocarriers were developed using acrylamide (AA), 2 hydroxyethyl methacrylate (HEMA), 3-(acryloyloxy)-2-hydroxypropyl methacrylate (AHM) [PAA-HEMA-AHM (NPs 1)], AA, 3-(aminopropyl) methacrylamide (APMA), and (+) N,N´-diallyl-L-tartardiamide (DAT) [PAA-APMA-DAT (NPs 2)] (**Fig. 1B)**. In addition, we evaluated the photoantimicrobial activity of the PSs loaded into novel PAA-NPs for application in APDT against methicillin-sensible Staphylococcus aureus (MSSA) and methicillin-resistant strains of S. aureus (MRSA). It has been reported that this bacterium is one of the most common microorganosm that is present in infected soft tissue lesions. Community and healthcare-acquired MRSA has dramatically increased [20,21].

Figure 1

2. Materials and Methods

2.1. Materials

NRBr and AzBBr were synthesized in our laboratory according to the procedure previously described [19,20].

AA, N,N,N´,N´-tetraethylmethylenediamine (TEMED), ammonium persulfate (APS), polyethylene glycol dodecyl ether (Brij 30), AHM, dioctyl sulfosuccinate (AOT), APMA, HEMA, DAT, and 9,10- anthracenediyl-bis (methylene)dimalonic acid (ABDA) were purchased from Sigma-Aldrich. Hexane, N,N-dimethylformamide (DMF), dimethylsulfoxide (DMSO), and ethanol were obtained from Sintorgan. Trypticase soy agar (TSA) was obtained from Britania (Buenos Aires, Argentina). Purification by dialysis was performed with cellulose ester membranes (MWCO 50 KDa; SpectrumLabs).

Phosphate-buffered saline (PBS, 10 mM pH 7.4) solution was prepared using sodium chloride, potassium chloride, sodium hydrogen phosphate dihydrate, and potassium dihydrophosphate. All the chemicals were of the highest purity commercially available (Cicarelli) and the solutions were prepared using ultrapure water from a Milli-Q® purification system.

2.2. Instrumentation

Absorption spectra were carried out at room temperature with a Cary 60 UV-Vis (Agilent Technologies) spectrophotometer between 200 and 800 nm using a 1 cm length quartz cell. All experiments were carried out at least twice with consistent results.

The average particle size, polydispersity index (PDI), and zeta potential (ZP) of the obtained NPs were evaluated using Dynamic Light Scattering (DLS) (Zetasizer Delsa Nano Version 2.20, Beckman Coulter Inc.). All measurements were carried out in triplicate at 25 ° C. The suspension of the NPs was appropriately diluted with Milli-Q water to attain suitable concentrations for analysis. The diameter and PDI of particle sizes were estimated using the CONTIN algorithm analysis through inverse Laplace Transformation of the autocorrelation function.

The pH was determined by a pH-meter (CRISON GLP 21) using a combined glass electrode.
The chemical stability of the dyes was evaluated using a thermostatic bath (Vicking®, Masson D).
Regarding the experiences with light, the samples were irradiated at a distance of 5 cm with a Parathom® lamp (OSRAM 5- W). The fluence rate measured with a Tes-1332 Digital Lux Meter (TES Electrical Electronic Corp.) was 8.4 mW/cm^2.

2.3. Synthesis of polyacrylamide nanoparticles

All NPs were prepared by inverse microemulsion polymerization. Hexane (12.5 mL) was added to a dried 50 mL reaction flask and stirred under a constant purge of nitrogen for 5 minutes. Suitable amounts of the surfactants AOT (0.533 g) and Brij 30 (1.033 g) were added to the reaction flask and stirring was continued under nitrogen protection for 20 min. The aqueous solution of appropriate monomers and crosslinkers (*see section 2.3.1.* or *2.3.2.*) for the different NPs was then added to the hexane reaction mixture and stirred at 500 rpm for another 20 min at 22 °C.
To initiate the polymerization reaction, 13.35 µL of APS aqueous solution (25 mg in 0.5 mL of Milli-Q water) and 13.35 µL of TEMED contained in 2.5 mL of hexane were added to the reaction mixture. The reaction was allowed to proceed for 1 day at room temperature.
Upon the completion of polymerization, hexane was removed by rotary evaporation and the particles were resuspended by addition of ethanol (15 mL).
Regarding the processing and preservation of the NPs, dialysis through special membranes (50 kDa) (3 days) was selected first in ethanol to remove the surfactant and residual monomers and then in water (3 days). The samples purified by dialysis were stored in a refrigerator at 4 °C.
DLS was employed to determinate the size of the NPs in aqueous solution.

2.3.1. Preparation of monomers and crosslinker solution to yield PAA-HEMA-AHM (NPs 1):
AA (monomer, 237 mg), HEMA (monomer, 20 µL), and AHM (crosslinker, 143 mg) were dissolved in phosphate buffered saline (0.67 mL) in a glass vial by sonication to obtain a uniform solution.
2.3.2. Preparation of monomers and crosslinker solution to yield PAA-APMA-DAT (NPs 2):
AA (monomer, 237 mg), APMA (monomer, 29.7 mg), and DAT (crosslinker, 152 mg) were dissolved in phosphate buffered saline (3.0 mL) in a glass vial by sonication to obtain a uniform solution.

2.4. Loading of nanoparticles with photosensitizers

The loading of the different nanoparticle systems, NPs 1 and NPs 2, with the PSs was made by post-synthesis modification of the NPs. To do this, 13.7 mL of Tween-80 was added to 1.37 mL (10 mg) of the NP solution. Then, different aliquots (in the range 100-500 µL) of the NRBr or AzBBr solution (1.3 mM) in DMSO were added to the NP solution and magnetically stirred at a constant rpm for at least 2 h. The excess of DMSO, Tween 80 and the PS that were not loaded, was removed by dialysis for 24 h.

2.5. Photodynamic properties: singlet oxygen determination

The use of ABDA in the detection of $^1O_2$ was first described by Lindig et al [22]. It has since been employed to assess $^1O_2$ generation by various photosensitiser systems.

ABDA reacts very rapidly and irreversibly with $^1O_2$ to produce an endoperoxide, resulting in the bleaching of the absorbance maximum of ABDA at approximately 380 nm [22, 23]. The endoperoxide formed is thermally stable at room temperature [24]. It is a useful method of quantification as, even when $^1O_2$ generation rates are low, the concentration of endoperoxide produced remains proportional to the cumulative amount of $^1O_2$ generated [25]. In addition, it has a high rate constant for reaction with $^1O_2$ and high water solubility, which allows testing in aqueous media, and in systems with biological applications [22, 26].

The solutions of ABDA (Absorbance 0.3) and the PS free and loaded into NPs (previously dialyzed) with an Absorbance of 0.2 in Milli-Q water were irradiated in 1 cm quartz cuvettes at 5 cm distance with a Parathom® lamp (OSRAM - 5 W) for a total time of 360 s. The kinetics of photooxidation of ABDA were studied by following the decrease of the absorbance (Abs) at λ_{max} = 380 nm as a function of irradiation time (**Fig. 2**). The photooxidation of ABDA was also used to determine the oxygen quantum yield (Φ_Δ) of the photosensitizers. The free forms of NRBr and AzBBr in aqueous solution were used as references (Φ_Δ= 1).

Figure 2

The observed rate constants (k_{obs}) were obtained by a linear least-squares fit of the plot of Abs versus time (**Fig. 3**).

The Φ_Δ of the dyes was calculated using **Eq. 1**, where PS is the photosensitizer, Ref is the reference compound, and Abs_0 is the initial absorbance of each PS at maximum absorption wavelengths. All determinations were carried out in triplicate.

$$\Phi_{\Delta}^{PS} = \frac{\Phi_{\Delta}^{Ref} k_{obs}^{PS} Abs_0^{Ref}}{k_{obs}^{Ref} Abs_0^{PS}} \quad \textbf{1.}$$

2.6. Stability and photostability tests

The chemical stability of the dyes was evaluated in buffer solutions at pH 7.4 at 37 °C by UV-visible spectroscopy and the samples were protected from light. The stock solutions of free dyes and NPs loaded with NRBr and AzBBr (previously dialyzed; 5 x 10^{-4} M) were prepared in buffer pH 7.4 prior to use. The standard solutions (25 mL; 3.5 x 10^{-5} M) of these compounds were prepared by diluting different aliquots of the corresponding stock solution with buffer pH 7.4. The samples were placed in a thermostatic bath. The aliquots were taken at different times and their Abs values were measured. The study was conducted for 6 h.

The photostability of free and loaded dyes (10^{-5} M) in buffer solution (pH 7.4) was carried out in quartz cells that were irradiated *(see section 2.2.)* at room temperature for 120 min (total light dose = 60.5 J/cm^2). It is important to note that the dye samples loaded into NPs were dialyzed before being measured. The solutions of the dyes were monitored by UV-visible spectroscopy as a function of time (**Fig. 4**). All stability studies were carried out in triplicate.

2.7. Antimicrobial Photodynamic Therapy studies

2.7.1. Bacterial strains and growth conditions

Methicillin-sensible *S. aureus* ATCC 29213 (MSSA) and methicillin-resistant *S. aureus* ATCC 43300 (MRSA) were used for this study. These strains were cultivated at 37 °C in TSA and maintained in this medium. An overnight culture was suspended in PBS and adjusted to a bacterial concentration of ~ 10^8 CFU/mL (corresponding to 0.5 Mc Farland scale). Finally, a 1/100 dilution of McFarland (cellular density: 10^6 CFU/mL) was prepared and used for the photodynamic inactivation assays.

2.7.2. Photodynamic inactivation of S. aureus in vitro.

The PSs were dissolved in a mixture of DMF: H_2O (1:9 v/v). The PAA-NPs were prepared as described in *section 2.3.* and then diluted with PBS to obtain solutions with the same concentration of the free dye and loaded form ([NRBr]: 18 µM and [AzBBr]: 15 µM). The DMF present in the final dilutions did not alter bacterial viability.

The aliquots of different PS solutions (1 mL) were transferred to a tube with 1 mL of 1/100 McFarland dilution. The cellular density used in the photodynamic assays was 10^6 CFU/mL and the final PS concentrations were 9 mM and 7.5 mM for NRBr and AzBBr, respectively. These suspensions were irradiated for 30 min and 15 min, reaching a total light dose of 15.1 J/cm^2 and 7.6 J/cm^2. Bacterial cultures grown under the same conditions with and without PS kept in the dark and illuminated cultures without sensitizer served as controls. When the lighting period ended, 100 µL aliquots were removed and serially diluted 10-fold. The number of viable bacteria was determined

in triplicate by the drop plate technique for bacterial enumeration according to Naghili et. al [27]. The CFU/mL was log-transformed and the PSs both free and loaded into NPs were compared with the control cultures. Statistics values were expressed as the mean ± standard deviation of each group. The difference between two means was compared by a two-tailed unpaired Student's t test. P values of < 0.05 were considered significant.

3. Results and Discussion

3.1. Synthesis, particle size, PDI, and zeta potential of polyacrylamide nanoparticles

In this study, our synthesis strategy focused on obtaining polyacrylamide nanoparticles with good characteristics. For this reason, we tested two pathways of synthesis (*see section 2.3.*). **Table 1** summarizes the size of the particles, PDI, and zeta potential values for the new nanoparticles, free and loaded with different dyes.

Table 1

According to these results, it can be said that the new PAA-NPs (NPs 1 and NPs 2) are optimal and present good size and acceptable PDI. These values allowed the conclusion that the NPs were distributed in only one population and were similar in size [28]. It is possible to affirm that the size of both nanoparticles increased with the vehiculization of NRBr and AzBBr, reaching 300 nm in all cases. These modifications demonstrated that there was an interaction between the different PAA-NPs and the PS.

The zeta potential of a nanoparticle is commonly used to characterize the surface charge property of NPs. It reflects the electrical potential of particles and is influenced by the composition of the particle and the medium in which it is dispersed. NPs with a zeta potential above ±30 mV have been shown to be stable in suspension, as the surface charge prevents the aggregation of the particles. The zeta potential can also be used to determine whether a charged active material is encapsulated within the center of the nanoparticle or on the surface [29, 30].

The value of zeta potential was found to be more than 30 mV for all NPs (**Table 1**). It indicates that the synthesized NPs could be expected to be stable for a longer time. Also, the zeta potential values varied from negative to positive when NRBr and AzBBr were loaded into PAA-NPs. This modification may be due to the fact that both dyes present cationic form (**Fig. 1**), which allows inferring that the PSs evaluated were located on the surface of the NPs.

3.2. Photodynamic properties: singlet oxygen determination

Fig. 3 A shows the kinetics of photooxidation of ABDA as a function of irradiation time for AzBBr loaded into NPs 1 and NPs 2. Similar results were obtained for the dye NRBr under the same experimental conditions (**Fig. 3 B**). From the analysis of these data, it was confirmed that both NPs

did not produce the oxidation of ABDA when they were irradiated. A similar behavior was observed for NRBr and AzBBr loaded into both systems and in the absence of light. Therefore, it is possible to state that the decomposition of ABDA is related to the formation of $^1O_2$, generated by the excitation of both PSs.

Figure 3

The values of the observed rate constant (k_{obs}) were obtained and Φ_Δ were calculated using **Eq. 1** These data for NRBr and AzBBr are summarized in **Table 2**.

Table 2

According to the obtained results, it is possible to affirm that for the PS of the family of azines (NRBr), the production of singlet oxygen increases considerably when this is loaded into the PAA-NPs in comparison with the free PS in water. Thus, the value of Φ_Δ for NPs 1-NRBr was 3.5 times greater than that obtained for the free NRBr, while, the value of Φ_Δ for NPs 2-NRBr tripled compared to the free PS.

On the other hand, a similar behavior was observed between AzBBr and NRBr when they were vehiculized. The vehiculization of the thiazine dyes caused greater decomposition of ABDA than the free one. However, no significant differences were observed in the $^1O_2$ production of both nanoparticle systems.

From the above, it can be deduced that the vehiculization of the dyes, NRBr and AzBBr, in PAA-NPs is able to optimize the photochemical properties of the PSs, which is an important advantage because they can be used in therapeutic applications.

These results are very promising and would indicate that the NPs of PAA have the capacity to induce the ROS generation of PSs and lead to the formation of more singlet oxygen at the action site.

3.3. Stability and photostability tests

Fig. 4 shows the chemical stability studies of the dye NRBr, free in water and loaded into PAA-NPs. The free dye NRBr was very unstable (half-time ($t_{½}$) = 10 min) in buffer solutions at pH 7.4. It was assayed at 37 °C for 6 h and followed a pseudo-first order kinetics. This fact means that at this pH the stability of NRBr was significantly affected. The results obtained demonstrated that the free dye AzBBr had a high chemical stability under the same experimental conditions tested for NRBr (data not shown).

Figure 4

However, when the studies were performed in the presence of both PAA-NPs, NPs 1 and NPs 2, the stability of the NRBr compound increased significantly and demonstrated to be stable during the 6 h

study period (**Fig. 4**). That is to say, the loading of the PS into the NPs protected them from chemical degradation.

On the other hand, in a previous work done by our research group, it was shown that the free dye NRBr presented high photostability [7]. However, AzBBr showed some photochemical instability ($t_{1/2}$ = 100 min) when assayed for 120 min. When this PS was loaded into both novel NPs the half-times remained essentially constant compared to the free dye. (data not shown).

It is possible to conclude that the vehiculization of both compounds in the new NPs presented a clear improvement in terms of their chemical and photochemical stability, which is a therapeutic advantage.

3.4. Inactivation of S. aureus in vitro.

In order to evaluate the effect of the vehiculization of NRBr and AzBBr in PAA-NPs on their photodynamic activity, the inactivation of MSSA and MRSA was tested *in vitro*. As shown in **Fig. 5,** the exposure of the bacteria to PSs free and encapsulated in NPs 1 and NPs 2 in the dark did not produce a reduction in CFU/mL. The same effect was observed when both strains of *S. aureus* were irradiated in the absence of the PSs. **Fig. 5 A** shows that the free NRBr, NPs 1-NRBr and NPs 2-NRBr caused a significant reduction in the Log CFU/mL of MSSA compared to the control solution. In addition, it was observed that after 30 min of irradiation the two nanoparticle systems produced a greater reduction in cell viability than the free PS, with no significant differences being observed between NPs 1-NRBr and NPs 2-NRBr.

When MRSA was treated with free and encapsulated NRBr, only the third generation PSs, NPs 1-NRBr and NPs2-NRBr, were observed to cause a significant reduction in the number of CFU/mL (**Fig. 5 B**). In contrast to MSSA, NPs 1- NRBr proved to be significantly better than NPs 2- NRBr in the inactivation of the resistant strain.

On the other hand, **Fig. 5 C** and **D** shows the photodynamic effect of AzBBr free and encapsulated in NPs (1 and 2) against MSSA and MRSA, respectively. In both cases, the third generation PSs caused a significant reduction in cell viability, with NPs 1-AzBBr being significantly better than free AzBBr and NPs 2-AzBBr. In fact, the maximum percentage of growth reduction was 35.5% (> 2 Log CFU/mL) with NPs 1-AzBBr against MRSA. It is important to note that the microorganisms treated with AzBBr were irradiated for 15 min because when they were exposed for 30 min to light, the percentage of death was 100%.

Figure 5

These results agree with those obtained in singlet oxygen production (*see section 3.2.*) because both PSs were more active when they were loaded into the NPs than when they were free. In turn, when

NPs 1 were used as carriers, the values obtained were better than when using NPs 2. These results make the third generation PSs good candidates for potential application in APDT.

4. Conclusions

Most efforts have been focused on developing novel low-complexity carriers that present an optimal synthesis route and can be loaded with PSs that produce ROS upon light activation and are stable during photodynamic action. The use of PAA-NPs as PS nanocarriers demonstrated to be a valuable tool to enhance the antimicrobial efficacy of the PSs and protect them from possible degradation under physiological conditions. The novel NPs presented ideal sizes and polydispersities.

The results obtained showed that the PSs, NRBr and AzBBr, can be successfully encapsulated in PAA-NPs and targeted against *S. aureus* without non-specific phototoxicity.

The encapsulation of both PSs in NPs 1 and 2 enhanced the size of the particles reaching 300 nm in all cases. The Φ_Δ increased considerably when the PSs were loaded into the NPs in comparison to the free PSs in water. The value of Φ_Δ for NPs 1-NRBr was 3.5 times greater than that obtained for the free NRBr, while the value of Φ_Δ for NPs 2-NRBr tripled compared to the free PS. The vehiculization of AzBBr in both PAA-NPs caused a similar increase in the decomposition of ABDA to that of the free PS.

This study describes experiments aimed at evaluating the efficiency of the novel systems, NPs 1 and NPs 2, in APDT. The two nanoparticle systems, NPs 1-NRBr and NPs 2-NRBr, produced a greater reduction in cell viability than the free PS, with no significant differences being observed between both systems in the methicillin-sensible strain. The NPs 1-NRBr caused a greater reduction in cell viability against MRSA than NPs 2-NRBr.

The dye AzBBr encapsulated in NPs 1 demonstrated to be better than NPs 2 against MSSA and MRSA.

It is possible to affirm that the vehiculization of NRBr and AzBBr in the PAA-NPs is able to optimize the photochemical properties of the PSs, which is an important advantage because they can be used in therapeutic applications.

Acknowledgments

This work was supported by grants from Secretaría de Ciencia y Técnica (SeCyT) 316/2016, Consejo Nacional de Investigaciones Científicas y Técnicas (CONICET) PIP N° 11220150100344CO, and Fondo para la Investigación Científica y Tecnológica (FonCyT). JV gratefully acknowledges receipt of a fellowship from CONICET. MSG, VA, and CIAI are career members of CONICET.

References .

[1] M. Managa, T. Nyokong, Photodynamic antimicrobial chemotherapy activity of gallium tetra-(4-carboxyphenyl) porphyrin when conjugated to differently shaped platinum nanoparticles, J. Mol. Struct. 1099 (2015) 432-440.

[2] O. Planas, R. Bresolí-Obach, J. Nos, T. Gallavardin, R. Ruiz-González, M. Agut, S. Nonell, Synthesis, Photophysical Characterization, and Photoinduced Antibacterial Activity of Methylene Blue-loaded Amino- and Mannose-Targeted Mesoporous Silica Nanoparticles, Molecules. 20 (2015) 6284-6298.

[3] M.R Hamblin, Antimicrobial photodynamic inactivation: a bright new technique to kill resistant microbes, Curr. Opin. Microbiol. 33 (2016) 67–73.

[4] T. Sung-Pin, H. Wei-Chun, C. Hsiao-Jan, L. Yu-Tzu, J. Hung-Sih, C. Hao-Chieh, H. Po-Ren, T. Lee-Jene, T. Jui-Chang, Effects of toluidine blue O (TBO)-photodynamic inactivation on communityassociated methicillin-resistant *Staphylococcus aureus* isolates, J. Microbiol. Immunol. 50 (2017) 46-54.

[5] M.N. Montes de Oca, J. Vara, L. Milla, V. Rivarola, C.S. Ortiz, Physicochemical properties and photodynamic activity of novel derivatives of Triarlylmethane and Thiazine, Arch. Pharm. Chem. Life Sci. 346 (2013) 255-265.

[6] M.N. Urrutia, C.S. Ortiz, Spectroscopic characterization and aggregation of azine compounds in different media, Chem. Physics. 412 (2013) 41–50.

[7] M.N. Urrutia, F.L. Alovero, C.S. Ortiz, New azine compounds as photoantimicrobial agents against *Staphylococcus aureus*, Dyes Pigments. 116 (2015) 27–35.

[8] R. Lei-Lei, C. Hong-Liang, X. Yu-Dong, L. Li-Chao, X. Lei, G. Yun, Z. Wei-An, Functional organic nanoparticles for photodynamic therapy, Chin. Chem. Lett. 27 (2016) 1412–1420.

[9] H. Abrahamse, M.R. Hamblin, New photosensitizers for photodynamic therapy, Biochem. J. 473 (2016) 347–364.

[10] X. Li, S. Kolemen, J. Yoon, E.U. Akkaya, Activatable Photosensitizers: Agents for Selective Photodynamic Therapy, Adv. Funct. Mater. 27 (2017) 1-11.

[11] S.S. Lucky, K.C. Soo, Y. Zhang, Nanoparticles in Photodynamic Therapy, Chem. Rev. 115 (2015) 1990−2042.

[12] S. Perni, P. Prokopovich, J. Pratten, I.P. Parkin, M. Wilson, Nanoparticles: their potential use in antibacterial photodynamic therapy, Photochem. Photobiol. Sci. 10 (2011) 712–720.

[13] M. Usacheva, B. Layek, S.S. Rahman Nirzhor, S. Prabha, Nanoparticle-Mediated Photodynamic Therapy for Mixed Biofilms, J. Nanomater, (2016) 1-11.

[14] C. Chueh-Pin, C. Chin-Tin, T. Tsuimin, Chitosan Nanoparticles for Antimicrobial Photodynamic Inactivation: Characterization and In Vitro Investigation, Photochem. Photobiol. 88 (2012) 570–576.

[15] T. Hopkins, R. Ukani, R. Kopelman, Intracellular Photodynamic Activity of Chlorin e6 Containing Nanoparticles, Int. J. Nanomed. Nanosurg. 2 (4) (2016) 1-4.

[16] T. Emre Yalcina, S. Ilbasmis-Tamera, B. Ibisoglub, A. Özdemirb, M. Arkb, S. Takkaa, Gemcitabine hydrochloride loaded liposomes and nanoparticles: Comparison of encapsulation efficiency, drug release, particle size and cytotoxicity, Pharm. Dev. Technol. DOI:10.1080/10837450. 2017.1357733.

[17] S. Nazzal , C. Chueh-Pin, T. Tsuimin, Nanotechnology in Antimicrobial Photodynamic Inactivation, J. Food Drug Anal. 19 (4) (2011) 383-395.

[18] M. Kuruppuarachchi, H. Savoie, A. Lowry, C. Alonso, R.W. Boyle, Polyacrylamide Nanoparticles as a Delivery System in Photodynamic Therapy, Mol. Pharmaceut. 8 (2011) 920-931.

[19] H. Kolya, T. Tripathy, Biodegradable flocculants based on polyacrylamide and poly(N,N-dimethylacrylamide) grafted amylopectin, Int. J. Biol. Macromol. 70 (2014) 26–36.

[20] K. Winkler, C. Simon, M. Finke, K. Bleses, M. Birke, N. Szentmáry, D. Hüttenberger, T. Eppig, T. Stachon, A. Langenbucher, F. Hans-Jochen, M. Herrmann, B. Seitz, M. Bischoff, Photodynamic inactivation of multidrug-resistant *Staphylococcus aureus* by chlorin e6 and red light, J. Photochem. Photobiol. B. 162 (2016) 340-347.

[21] T.A. Skwor, S. Klemm, H. Zhang, B. Schardt, S. Blaszczyk, M.A. Bork, Photodynamic inactivation of methicillin-resistant *Staphylococcus aureus* and *Escherichia coli*: A metalloporphyrin comparison. J. Photochem. Photobiol. B. 165 (2016) 51–57.

[22] B. Lindig, M. Rodgers, A. Schapp, Determination of the lifetime of singlet oxygen in water-d2 using 9,10-anthracenedipropionic acid, a water-soluble probe, J. Am. Chem. Soc. 102 (1980) 5590–5593.

[23] C. Xing, Q. Xu, H. Tang, L. Liu, S. Wang, Conjugated polymer/porphyrin complexes for efficient energy transfer and improving light-activated antibacterial activity, J. Am. Chem. Soc. 131 (2009) 13117–13124.

[24] M. Moreno, E. Monson, R. Reddy, A. Rehemtulla, B. Ross, M. Philbert, Production of singlet oxygen by $Ru(dpp(SO_3)_2)_3$ incorporated in polyacrylamide PEBBLES, Sens. Actuators B. 90 (2003) 82–89.

[25] Y. Cao, Y. Koo, S. Koo, R. Kopelman, Ratiometric Singlet Oxygen Nano-optodes and Their Use for Monitoring Photodynamic Therapy Nanoplatforms, Photochem. Photobiol. 81 (2005) 1489–1498.

[26] B. Lindig, M. Rodgers, Rate Parameters For The Quenching of Singlet Oxygen by Water Soluble and Lipid-Soluble Substrates in Aqueous and Micellar Systems, Photochem. Photobiol. 33 (1981) 627–634.

[27] H. Naghili, H. Tajik, K. Mardani, S.M. Razavi Rouhani, A. Ehsani, P. Zare, Validation of drop plate technique for bacterial enumeration by parametric and nonparametric tests, Vet. Res. Forum. 4 (3) (2013) 179–183.

[28] R.J. Lancheros, J.A. Beleño, C.A. Guerrero, R.D. Godoy-Silva, Producción de Nanopartículas de PLGA por el método de emulsión y evaporación para encapsular N-Acetilcisteina (NAC). Universitas Scientiarum. 19 (2014) 161-168.

[29] R. Singh, J.W. Lillard Jr, Nanoparticle-based targeted drug delivery, Exp. Mol. Pathol. 86 (2009) 215-223.

[30] S. Honary, F. Zahir, Effect of Zeta Potential on the Properties of Nano-Drug Delivery Systems - A Review (Part 2), Trop. J. Pharm. Res. 12 (2013) 265-273.

[31] M.S. Gualdesi, C.I. Alvarez Igarzabal, J. Vara, C.S. Ortiz, Synthesis and physicochemical properties of polyacrylamide nanoparticles as photosensitizer carriers, Int. J. Pharm. 512 (2016) 213-218.

Figure 1. A. Chemical structure of PSs. **B.** Synthesis of new PAA-NPs.

Figure 2. UV-Visible absorbance spectra of ABDA in solution with NPs 1-AzBBr irradiated at different times (in the range 0-360 s).

Figure 3. Kinetics of photooxidation of ABDA at λ_{max}=380 nm as a function of irradiation time for AzBBr (**A**) and NRBr (**B**) in different PAA-NPs.

Figure 4. Stability studies of free NRBr in water and loaded into PAA-NPs.

Figure 5. Photodynamic inactivation of MSSA (**A** and **C**) and MRSA (**B** and **D**) treated with different PSs.

Table 1. Particles size, PDI, and zeta potential values for new NPs, free and loaded with different dyes.

Characteristics	Free PAA-NPs		PAA-NPs-NRBr[a]		PAA-NPs-AzBBr[b]	
	NPs 1	NPs 2	NPs 1	NPs 2	NPs 1	NPs 2
Average size (nm)	94.3	91.5	298	303	294	307
Zeta potential (mV)	-35	-32	+30	+37	+31	+33
PDI	0.25	0.23	0.24	0.27	0.25	0.26

a and b: aliquot of 100 µL of stock solution 20 mM.

Table 2. Kinetic parameters for the photooxidation and Φ_Δ of NRBr and AzBBr, free and loaded into NPs.

PS	Absorbance*	$-k_{obs}$* ($x10^{-4}$; s^{-1})	Φ_Δ
Free NRBr	0.226±0.025	0.5±0.1	1
NPs 1-NRBr	0.245±0.002	2.0±0.1	3.46
NPs 2-NRBr	0.202±0.001	1.9±0.1	3.02
Free AzBBr	0.195±0.004	9.6±0.2	1
NPs 1-AzBBr	0.160±0.008	9.6±0.3	1.22
NPs 2-AzBBr	0.131±0.003	7.8±0.1	1.21

*Determination number, n = 3

Highlights

- Polyacrylamide nanoparticles were synthesized and charectizarated.
- Singlet oxygen and chemical stability determination of dyes were studied.
- Antimicrobial photodynamic therapy against *S. aureus* was evaluated.

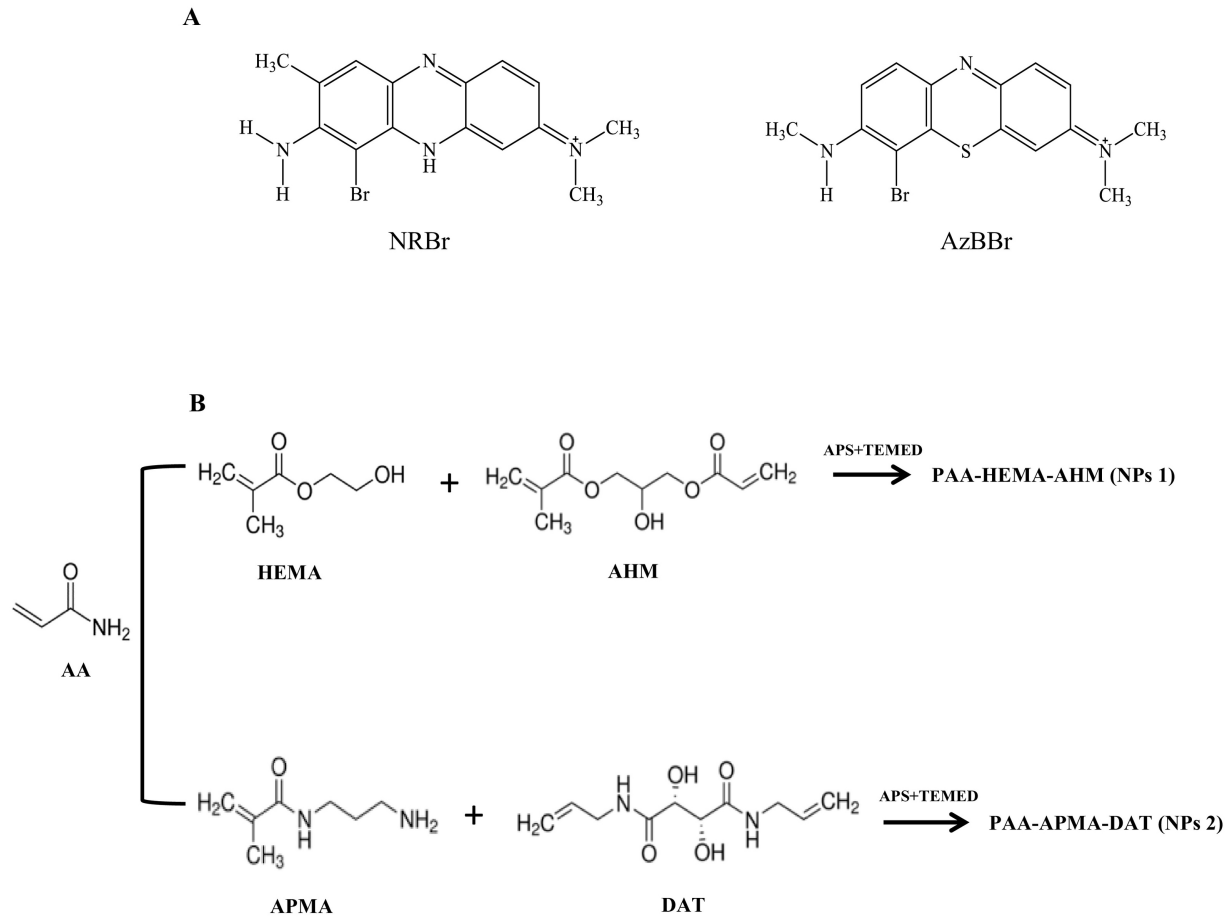
A
NRBr
AzBBr
B
HEMA
AHM
APS+TEMED
PAA-HEMA-AHM (NPs 1)
AA
APMA
DAT
APS+TEMED
PAA-APMA-DAT (NPs 2)

Figure 1

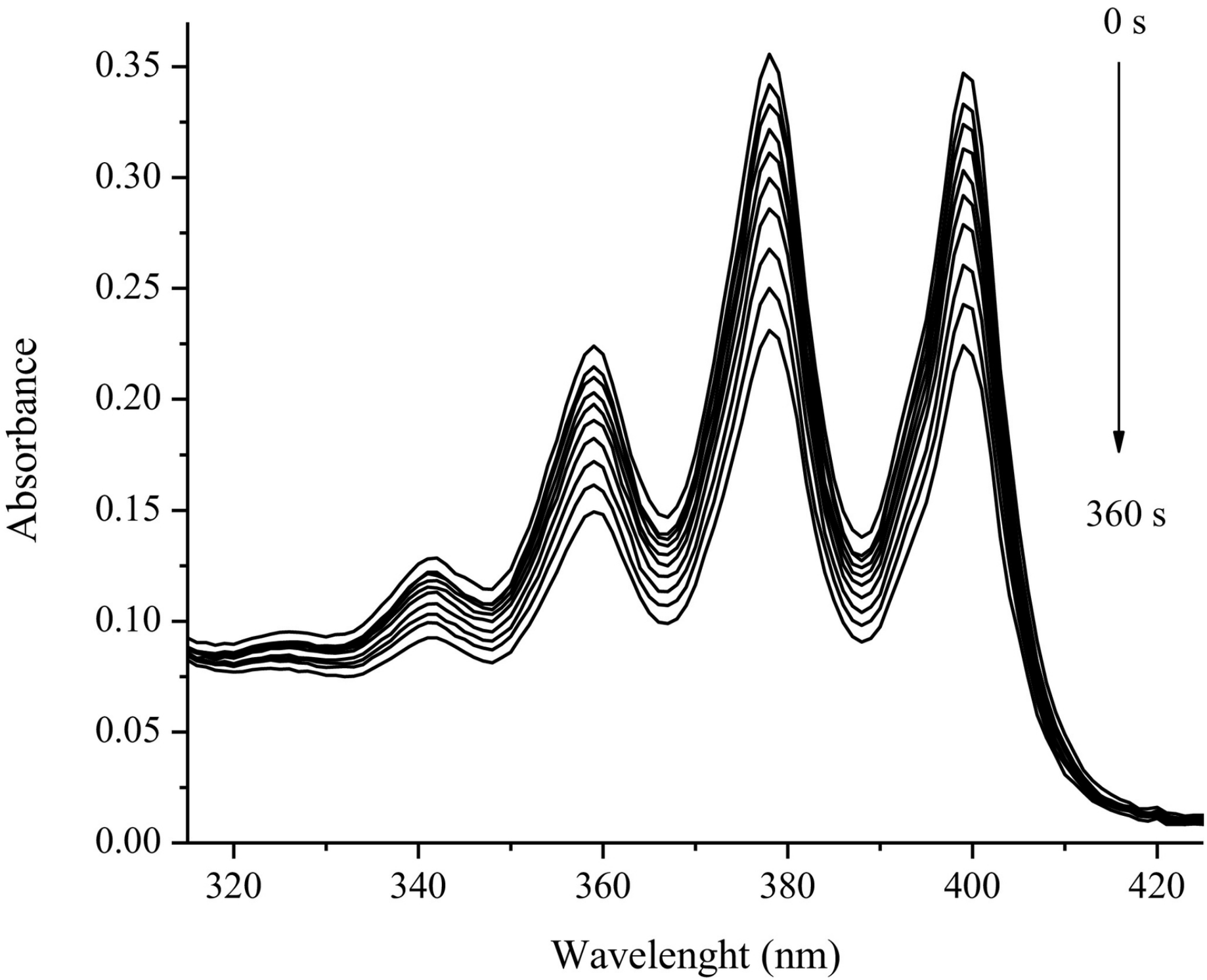
0 s
360 s
Absorbance
0.35
0.30
0.25
0.20
0.15
0.10
0.05
0.00
320
340
360
380
400
420
Wavelenght (nm)

Figure 2

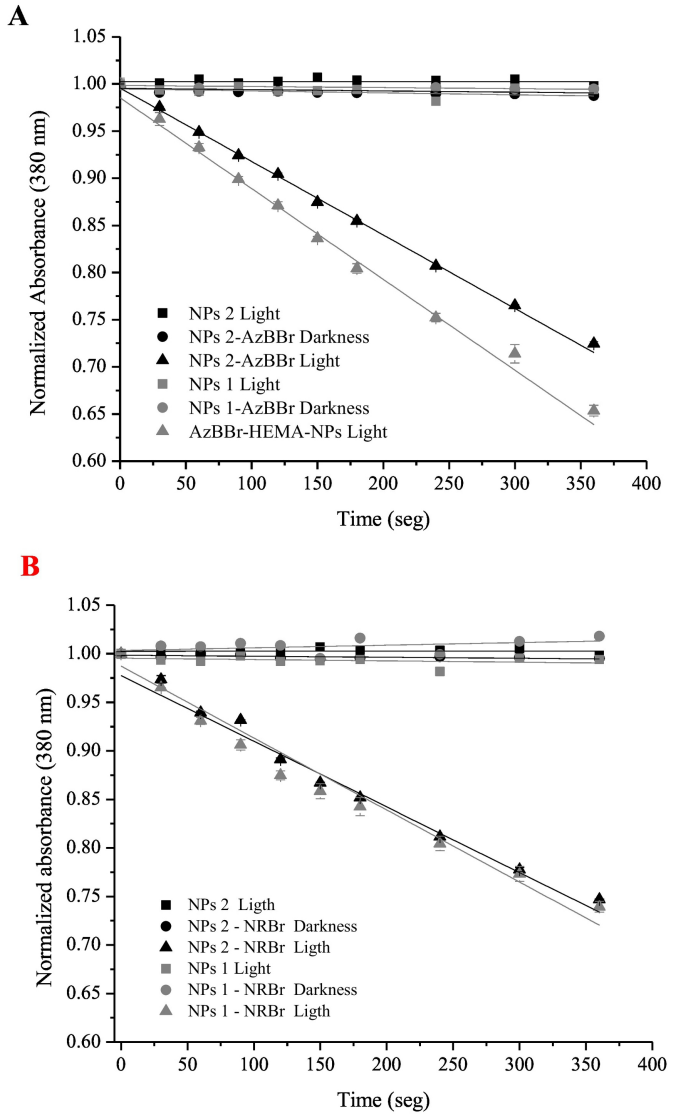
A
Normalized Absorbance (380 nm)
Time (seg)
NPs 2 Light
NPs 2-AzBBr Darkness
NPs 2-AzBBr Light
NPs 1 Light
NPs 1-AzBBr Darkness
AzBBr-HEMA-NPs Light
B
Normalized absorbance (380 nm)
Time (seg)
NPs 2 Ligth
NPs 2 - NRBr Darkness
NPs 2 - NRBr Ligth
NPs 1 Light
NPs 1 - NRBr Darkness
NPs 1 - NRBr Ligth

Figure 3

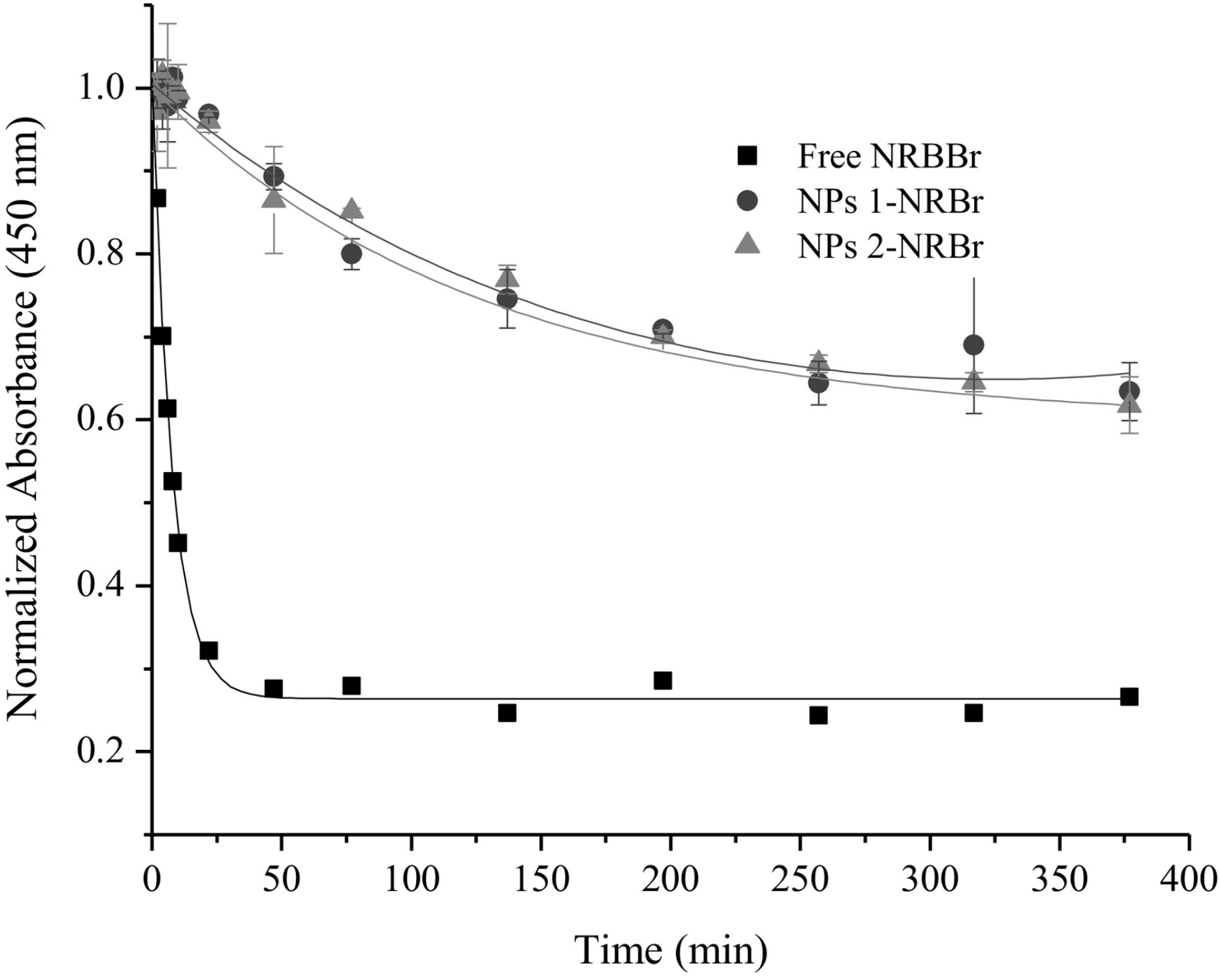
Normalized Absorbance (450 nm)
1.0
0.8
0.6
0.4
0.2
0
50
100
150
200
250
300
350
400
Time (min)
Free NRBBr
NPs 1-NRBr
NPs 2-NRBr

Figure 4

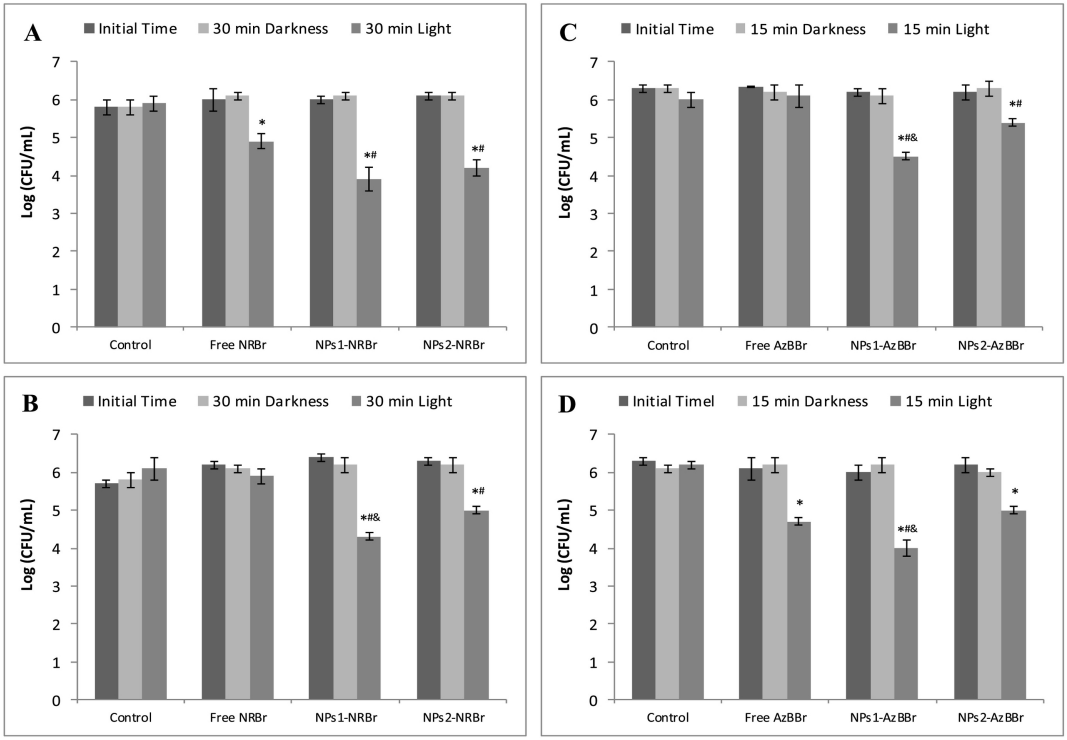
A
Initial Time
30 min Darkness
30 min Light
Log (CFU/mL)
Control
Free NRBr
NPs1-NRBr
NPs2-NRBr
C
Initial Time
15 min Darkness
15 min Light
Log (CFU/mL)
Control
Free AzBBr
NPs1-AzBBr
NPs2-AzBBr
B
Initial Time
30 min Darkness
30 min Light
Log (CFU/mL)
Control
Free NRBr
NPs1-NRBr
NPs2-NRBr
D
Initial Timel
15 min Darkness
15 min Light
Log (CFU/mL)
Control
Free AzBBr
NPs1-AzBBr
NPs2-AzBBr

Figure 5